OPEN ACCESS
Advances in Complex Systems
Vol. 28, No. 6 (2025) 2540006 (21 pages)

DOI: 10.1142/S0219525925400065

DYNAMIC MODELS OF GENTRIFICATION

GIOVANNI MAURO ‡
ISTI-CNR, Pisa, Italy
Scuola Normale Superiore, Pisa, Italy
Department of Computer Science, University of Pisa, Pisa, Italy
IMT School for Advanced Studies, Lucca, Italy
giovanni.mauro@sns.it

NICOLA PEDRESCHI * and RENAUD LAMBIOTTE †
Mathematical Institute, University of Oxford, UK
**nicola.pedreschi@maths.ox.ac.uk*
†*renaud.lambiotte@maths.ox.ac.uk*

LUCA PAPPALARDO
ISTI-CNR, Pisa, Italy
Scuola Normale Superiore, Pisa, Italy
luca.pappalardo@isti.cnr.it

Received 4 January 2025
Revised 14 April 2025
Accepted 4 June 2025
Published 28 July 2025

The phenomenon of gentrification of an urban area is characterized by the displacement of lower-income residents due to rising living costs and an influx of wealthier individuals. This study presents an agent-based model that simulates urban gentrification through the relocation of three income groups — low, middle, and high — driven by living costs. The model incorporates economic and sociological theories to generate realistic neighborhood transition patterns. We introduce a temporal network-based measure to track the outflow of low-income residents and the inflow of middle- and high-income residents over time. Our experiments reveal that high-income residents trigger gentrification and that our network-based measure consistently detects gentrification patterns earlier than traditional count-based methods, potentially serving as an early detection tool in real-world scenarios. Moreover, the analysis highlights how city density promotes gentrification. This framework offers valuable insights for understanding gentrification dynamics and informing urban planning and policy decisions.

Keywords: Gentrification; urban dynamics; temporal networks.

‡ Corresponding author.

1. Introduction

Cities are dynamic systems [7, 20, 41] in which the interactions between numerous agents determine the emergence of non-trivial patterns at different scales, such as traffic congestion, [10] epidemic spreading [30, 38], and socioeconomic segregation [12, 35, 46]. Gentrification, first defined by Ruth Glass in 1964 [14], describes the transformation of neighborhoods from working-class to affluent areas, often displacing original residents, and potentially undermining urban diversity and affordability [20]. Slater [49] divides gentrification research into two main strands: production-side and consumption-side theories. Both reject the view that gentrification is a benign return to urban centers [25, 27], with production-side theories linking it to economic factors such as the rent gap [50, 51] and housing quality decline [29]. Conversely, consumption-side theories emphasize the growing appeal of city centers [48], where proximity to urban amenities fuels demand. Ley [26] argues that artists, drawn by the cultural and social vitality of these areas, act as early catalysts for gentrification, eventually attracting wealthier residents and driving up property values [16].

Computational studies have blurred the lines between these perspectives, focusing on housing market dynamics, particularly fluctuations in rent and housing prices, as these reflect the real-world data used to validate their models. O'Sullivan [39] proposes a model incorporating housing markets, social networks, history, and policies, illustrating how gentrification operates in cycles influenced by these factors. Redfern [44] introduces the "investment gap," emphasizing the difference between non-modernized homes and their potential if modernized, with domestic technologies driving gentrification. Other computational models simulate household movements [28], considering vacancies, accessibility, socioeconomic status, and urban policies [11, 53]. Alternatively, machine learning approaches have been implemented in an attempt to predict gentrification events [43, 45], in some limited cases taking into account proxies for human mobility in urban areas [13]. A recent work by Shaw *et al.* [47] showed how even a simple dynamical system model of gentrification, focused on neighborhood attractiveness and artist populations, can generate complex temporal patterns including synchronized oscillations and transient chaos.

In this study, we present an agent-based model of gentrification, inspired by the work of Schelling on urban segregation [46]. Rather than focusing on replicating housing market dynamics, we base our analysis of gentrification on the relocation flows of citizens in a stylized urban grid. Our model is founded on the key assumption that gentrification is driven by socioeconomic inequality and additionally by differing relocation strategies across income levels. As Nieuwenhuis *et al.* [36] found, in high-inequality contexts, low-income groups are confined to deprived areas while high-income groups maintain spatial dominance, creating a "vicious circle" that perpetuates inequality. Based on further insights from the literature [3, 8, 19], we assume that agents relocate according to their socioeconomic conditions [31]: low-income agents move when priced out of a neighborhood, medium-income agents gravitate toward areas with similar economic conditions and quality of life, while high-income

agents are attracted to areas undergoing economic growth where they can maximize investment returns. These contrasting behaviors, along with a heavy-tailed income distribution, are the only drivers of neighborhood transformations. While our agent-based model builds on simple rules, it generates complex and emergent dynamics, requiring a rigorous complex systems approach to quantify and interpret the multifaceted aspects of gentrification.

Within our modeling framework, we show that gentrification emerges only when high-income residents have some mobility, even if minimal, highlighting how their movement patterns catalyze the process. We treat relocation flows of agents in our city as time-varying edges in a temporal network [15, 32], leveraging established tools from network science and human mobility research [4, 33, 37, 40, 41]. We introduce two novel measures to quantify gentrification within our theoretical framework. The first measure translates the conventional definition of gentrification into a metric based on the over-representation of middle- and high-income agents in a given area. The second measure captures the dynamics of gentrification by tracking the inflow of these agents alongside the simultaneous outflow of low-income residents. Our findings demonstrate that this dynamic measure can consistently detect gentrification earlier than the more intuitive, count-based approaches, making it a potential early-warning indicator for policymakers aiming to mitigate its impacts. Additionally, our framework can simulate the effects of various urban planning strategies and city characteristics on gentrification. Notably, we observe a direct correlation between urban density and the frequency of gentrification events. Overall, our model and measures offer a comprehensive perspective on gentrification, shedding new light on this complex urban phenomenon.

2. Agent-based Model of Gentrification

2.1. *Modeling the city and its citizens*

We model the urban environment as a 77 grid, with each cell representing a city neighborhood (Fig. 1(a)). We populate this grid with 2^{12} agents, categorized into three socioeconomic groups: low-income (L), middle-income (M), and high-income (H). At the beginning of a simulation, each agent is assigned a fixed income w, sampled from real-world data, and all agents are divided into three groups according to their assigned incomes: L accounting for 38% of the population; M accounting for 57% of the population; and H corresponding to the remaining 5% of the population of the model city. The method of income assignment is based on data from the 2022 USA Social Security Administration report [52] (see Sec. 6 for further details) and allows income variation within each agent class. Figure 1(b) shows one realization of income assignment to the agents resulting in a heavy-tailed agent income distribution (more details in Sec. 6).

The spatial distribution of the agents follows a socioeconomic radial gradient: H agents predominantly occupy the city center, M agents populate the inner areas, and

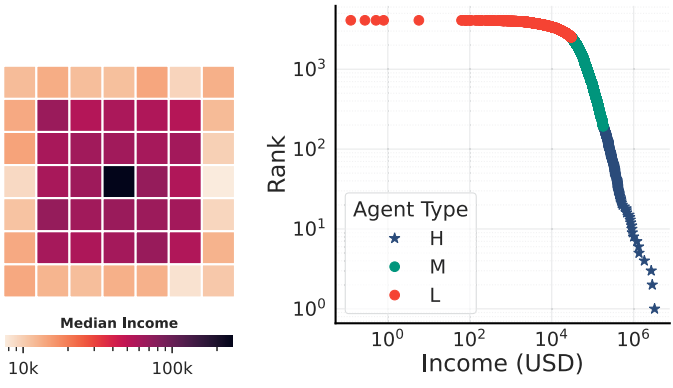

(a) (b)

Fig. 1. (Color online) Income and spatial distribution: (a) Heatmap reporting the median income of each cell at the beginning of a simulation. The darker the color, the higher the median income of the cell. (b) Log–log plot of the Initial distribution of the income, sampled from the 2022 USA Social Security Administration report [52], of the agents in a simulation with $N = 2^{12}$ agents.

L agents are concentrated in the periphery (Fig. 1(a)). This mono-centric structure reflects the presence of a dominant central business district, found in many cities or metropolitan areas of varying sizes [2, 6]. Each cell (neighborhood) j has a fixed maximum capacity K, which limits its occupancy, that is, how many agents can stay there. When $n(j)$, the number of agents in the cell j, reaches maximum capacity K, agents are allocated to the nearest available locations. Our model operates based on two key parameters: the parameter p_H that corresponds to the probability that a H agent relocates from its current cell to a new one where the median agent-income is increasing; the parameter θ that is the width of the time window over which H agents evaluate cell growth trends. Our model simulates a 7×7 grid city comprising 49 neighborhoods, a scale consistent with moderately large urban areas. To ensure the robustness of our findings, we extended our analysis to an even larger urban environment (9×9 grid, 81 neighborhoods), as well as to a city with maximally mixed distribution of agents of the three types, where the radial gradient of income is lost, obtaining similar results (see Supplementary Information 3–5).

2.2. *Agent relocation dynamics*

Our model implements income-dependent relocation rules for three agent classes across a set of cells, where each cell i has a maximum capacity K. Let $n(i)$ denote the number of agents in cell i at any given time. Figures 2(a)–2(f) illustrate the rules behind agents' behaviors.

An L agent is likely to move away from a cell if they are significantly poorer than other agents in the cell. The agent moves, with higher probability, to a cell where the income gap with current residents is smaller. The probability of an L agent leaving

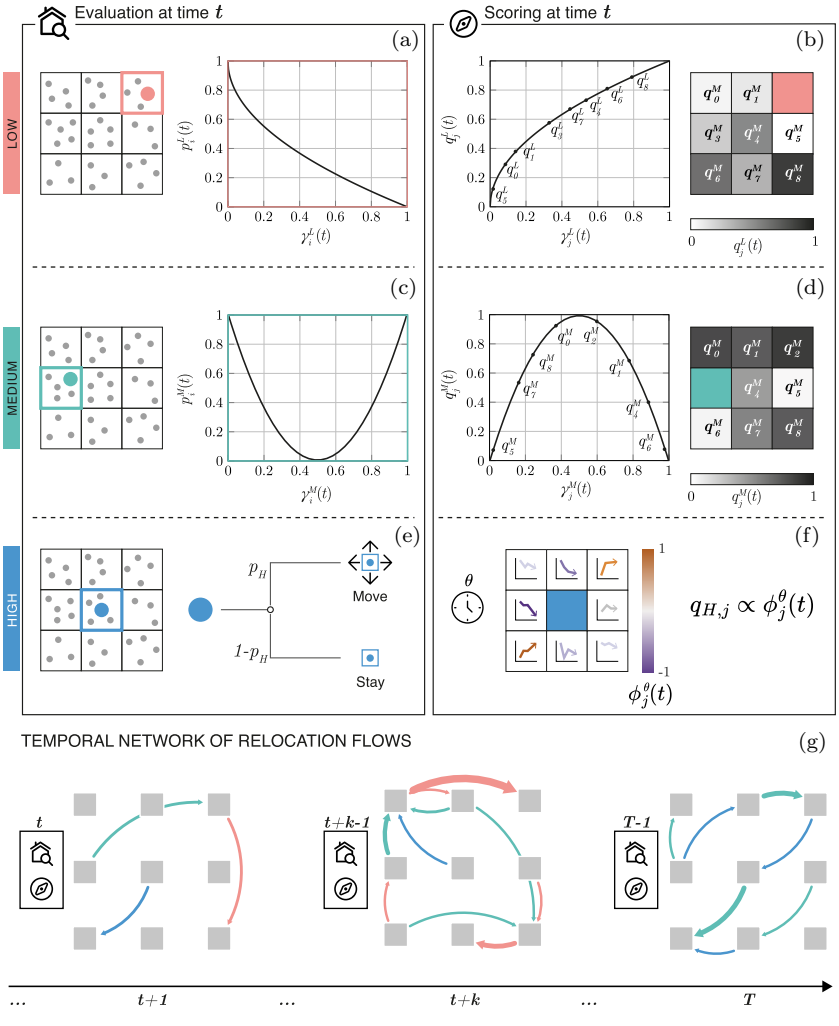

Fig. 2. (Color online) Income-profile-specific agent behavior: The city is represented as a grid at time t, with three types of agents distributed across the cells. We track a low-income agent L (red cell), a middle-income agent M (green cell), and a high-income agent H (blue cell). (a) The L agent moves from its current cell i with a probability $p_i^L(t)$, which is inversely proportional to its income percentile in i. (b) When L moves, it relocates to a new cell j with probability $q_j^L(t)$. (c) The M agent moves from its current cell i with probability $p_i^M(t)$, that its higher the more the income percentile of M is extreme. (d) When M moves, it relocates to a new cell j with probability $q_j^M(t)$. (e) The H agent moves with a fixed probability p_H. (f) The H agent moves to a new cell j based on its growth rate $\phi_j^\theta(t)$. At time $t+1$, the L agent moves to cell $j=8$, the M agent to cell $j=2$, and the H agent to cell $j=6$. (g) The output of our model is a temporal network, where nodes are grid cells and edges represent agent flows between cells over time. The first snapshot of the network at $t+1$ shows the flows generated by (a)–(f). The model stops when no L agent can move, resulting in no red edges in the final network snapshot at time T.

cell i at time t, shown in Fig. 2(a), is given by

$$p_i^L(t) = 1 - \gamma_i^L(t)^{\frac{1}{2}}, \tag{1}$$

where $\gamma_i^L(t) \in (0, 1]$ represents the agent's relative income percentile within cell i's income distribution at time t. Upon deciding to move, L agents select from the set $\mathcal{J}$ of available cells, defined as cells where $n(j) < K$. As illustrated in Fig. 2(b), the probability of selecting cell j is

$$\rho_j^L(t) = \frac{q_j^L(t)}{\sum_{n\in\mathcal{J}} q_n^L(t)}, \quad q_j^L(t) = \gamma_j^L(t)^{\frac{1}{2}}, \tag{2}$$

where $q_j^L(t)$ is the cell's attractiveness score based on the agent's prospective income percentile in cell j.

An M agent is likely to move away when its income significantly deviates from the median income in the current cell. The agent will move to a cell where the gap with the median income is lower. Their relocation probability, visualized in Fig. 2(c), follows:

$$p_i^M(t) = 4(\gamma_i^M(t) - 0.5)^2, \tag{3}$$

where $\gamma_i^M(t) \in [0, 1]$ is the M agent's relative income percentile in cell i. Figure 2(d) shows how their destination selection probability is determined by

$$\rho_j^M(t) = \frac{q_j^M(t)}{\sum_{n\in\mathcal{J}} q_n^M(t)}, \quad q_j^M(t) = 1 - 4(\gamma_j^M(t) - 0.5)^2, \tag{4}$$

where $q_j^M(t)$ scores cells based on proximity to their median income.

For both L and M agents, we choose nonlinear functional forms (square root for L, quadratic for M) to ensure that small differences in percentiles lead to larger differences in probabilities when agents are far from their preferred positions. The denominators in $\rho_j^L(t)$ and $\rho_j^M(t)$ serve as normalization factors, ensuring proper probability distributions.

A H agent moves from its current cell i with a fixed probability $p_H \in [0, 1]$. Let $\tilde{w}_j(t)$ denote the median income in cell j at time t. H agents select from set $\mathcal{H}$ of cells satisfying both $n(j) < K$ and $\phi_j^\theta(t) > \phi_i^\theta(t)$, where $\phi_j^\theta(t)$ is the average growth rate of median income over the past θ time steps, as reported in Figs. 2(e) and 2(f):

$$\phi_j^\theta(t) = \frac{1}{\theta} \sum_{\tau=t-\theta}^{t} [\tilde{w}_j(\tau) - \tilde{w}_j(\tau - 1)]. \tag{5}$$

Their destination probability is

$$q_j^H(t) = \frac{\phi_j^\theta(t)}{\sum_{n\in\mathcal{H}} \phi_n^\theta(t)}. \tag{6}$$

The definition of the destination probability $q_j^H(t)$ reflects the profit-orientated nature of the movement of H agents. Cells that underwent a higher growth in the last Θ

steps are thus more likely to be selected as destination. To ensure an easier interpretation of the results of our model, we impose that H agents do not operate (move) in the first θ steps, i.e. until a full evaluation of the growth-rate $\phi^{\theta}(t)$ of cells has been completed. The simulation terminates at time T when all L agents can only find cells that would place them in the lowest income percentile, or after 300 time steps. We denote the termination time as T. All simulations were implemented using the Python library `mesa` [22]. The complete source code for model implementation and experimental procedures is available at: https://github.com/mauruscz/Gentrification

3. Measures of Gentrification

Our gentrification model generates dynamic flows of agents of the three types among grid cells (see Fig. 2(g)). We model these time-varying flows as a dynamic network where nodes represent grid cells and edges correspond to movements of agents of the three types. The network consists of three layers, each representing flows of L, M, or H agents. This representation results in a temporal network [17, 18, 32], which is multi-layer (one per each edge type) [23] and weighted [5], defined as follows:

$$\mathrm{G}^{\alpha}(t) = \{A^{\alpha}_{i,j}(t) | i, j \in V; \alpha \in \{L, M, H\}; t \in [0, T]\}, \tag{7}$$

where V denotes the set of nodes (grid cells) in the network, α represents the layer index corresponding to L, M or H agents, and $A^{\alpha}(t)$ is the adjacency matrix corresponding to the network in layer α at time t. The matrix elements of $\mathbf{A}^{\alpha}(t)$ correspond to weighted, directed edges connecting node pairs in layer α, representing the relocation flows of agents of type α between contiguous time steps of the agent-based model. For each layer $\alpha \in [L, M, H]$ at time t, we define three quantities: $n^{i}_{\alpha}(t)$, the number of agents in node i, and $s^{\mathrm{in}}_{i,\alpha}(t)$ and $s^{\mathrm{out}}_{i,\alpha}(t)$, the in- and out-strength of node i, respectively. The latter two quantify the flow of agents in $[L, M, H]$ moving to or from node i between $t-1$ and t:

$$\begin{aligned} s^{\mathrm{in}}_{i,\alpha}(t) &= \sum_{i} A^{\alpha}_{i,j}(t), \\ s^{\mathrm{out}}_{i,\alpha}(t) &= \sum_{j} A^{\alpha}_{i,j}(t), \\ \alpha &= L, M, H, \end{aligned} \tag{8}$$

where $A^{\alpha}_{i,j}(t)$ represents the (i, j) element of the weighted adjacency matrix for layer α at time t.

In the following subsections, we introduce two complementary metrics to capture the dynamics of gentrification. The first metric adopts a "migration stock" perspective [1], aiming to formalize the typical definition found in the social science literature, which largely emphasizes changes in neighborhood composition over time. These definitions [14, 26, 51] generally focus on the transformation of a place, such as the increasing presence of higher-income residents, rather than on the movement of

people itself. To complement this, the second metric takes a "migration flow" perspective [1], shifting attention to the dynamics of displacement. It specifically measures the number of L agents who leave a place as a result of being pushed out by incoming M and H agents.

3.1. *Count-based measure*

Gentrification is often defined as a period in which a neighborhood (a cell in the grid and a node in the temporal network), previously populated by a majority of lower-income citizens, undergoes a gradual replacement of its population with middle- and higher-income citizens [14, 20]. To capture this process, we introduce a measure of gentrification for each node in the network, denoted as $\mathcal{G}^i_{\text{count}}(t, \Delta)$, based on the number of agents from each socioeconomic class present in node i at two time points: the current time t and an earlier time $t - \Delta$. For each time point, we consider the counts of H, M and L agents. At time t, these counts are represented by $n^i_H(t)$, $n^i_M(t)$, and $n^i_L(t)$, respectively. Similarly, at time $t - \Delta$, the counts are denoted by $n^i_H(t - \Delta)$, $n^i_M(t - \Delta)$, and $n^i_L(t - \Delta)$. The definition of $\mathcal{G}^i_{\text{count}}(t, \Delta)$ is as follows:

$$\mathcal{G}^i_{\text{count}}(t, \Delta) = \frac{1}{\Delta} \sum_{\tau=t-\Delta}^{t} \frac{n^i_H(\tau) + n^i_M(\tau)}{n^i_H(\tau) + n^i_M(\tau) + n^i_L(\tau)} \tag{9}$$

$\mathcal{G}^i_{\text{count}}(t, \Delta)$ represents the average fraction of H and M agents in node i over the time window $[t - \Delta, t]$. We establish a significance threshold $n^*_{H,M}$, defined as the expected node-wise fraction of H and M agents under uniform random distribution across the grid. Values of $\mathcal{G}^i_{\text{count}}(t, \Delta)$ exceeding $n^*_{H,M}$ indicate an over-representation of H agents. Gentrification is identified when $\mathcal{G}^i_{\text{count}}(t, \Delta)$ transitions from below to above this threshold. This metric functions as a node property, independent of the network edge dynamics.

To identify gentrification, we establish a critical threshold $n^*_{M,H} = 0.62$, representing the city-wide proportion of M and H agents. To precisely capture gentrification events, we introduce the binary indicator $\mathcal{G}_{\text{bin}}$:

$$\mathcal{G}_{\text{bin}}(t, \Delta) = \begin{cases} 1, & \text{if } \mathcal{G}_{\text{count}}(t, \Delta) > n^*_{H,M}, \\ 0, & \text{otherwise.} \end{cases} \tag{10}$$

We define t_{shift}, the onset of a gentrification event, as the moment when $\mathcal{G}_{\text{bin}}$ shifts from 0 to 1, indicating that a neighborhood has crossed the critical M, H population threshold. More mathematical details about t_{shift} can be found in Sec. 6.

3.2. *Network-based measure*

The count-based measure, while providing an intuitive quantification of gentrification, has notable limitations: it requires a significance threshold and only detects completed transitions, disregarding inter-neighborhood dynamics. To overcome these constraints, we define a gentrification measure based on the temporal

relocation network, $\mathcal{G}^i_{\text{net}}(t, \Delta)$ that captures relocation patterns between neighborhoods. For any node i in the network, this measure considers the net-outflow of L agents, $\varphi^{\text{out}}_i(t)$, and the net-inflow of M and H agents, $\varphi^{\text{in}}_i(t)$:

$$\varphi^{\text{out}}_i(t) \equiv \frac{s^{\text{out}}_{i,L}(t) - s^{\text{in}}_{i,L}(t)}{s^{\text{out}}_{i,L}(t) + s^{\text{out}}_{i,M}(t) + s^{\text{out}}_{i,H}(t)}, \tag{11}$$

$$\varphi^{\text{in}}_i(t) \equiv \frac{s^{\text{in}}_{i,M,H}(t) - s^{\text{out}}_{i,M,H}(t)}{s^{\text{in}}_{i,L} + s^{\text{in}}_{i,M}(t) + s^{\text{in}}_{i,H}(t)}, \tag{12}$$

where $s^{\text{in}}_{i,M,H}(t) = s^{\text{in}}_{i,M}(t) + s^{\text{in}}_{i,H}(t)$ and $s^{\text{out}}_{i,M,H}(t) = s^{\text{out}}_{i,M}(t) - s^{\text{out}}_{i,H}(t)$.

$\varphi^{\text{out}}_i(\tau)$ is high when the outflow of L agents from node i corresponds to a high fraction of the overall outflow of agents from i, i.e. the denominator in Eq. (11); $\varphi^{\text{in}}_i(\tau)$ is high when the inflow of M and H agents to node i corresponds to a high fraction of the overall inflow of agents toward i, i.e. the denominator in Eq. (12). $\mathcal{G}^i_{\text{net}}(t, \Delta)$ is therefore defined as the geometric mean of the averages of $\varphi^{\text{out}}_i(t)$ and $\varphi^{\text{in}}_i(t)$ over the last steps Δ:

$$\mathcal{G}^i_{\text{net}}(t, \Delta) \equiv \sqrt{\left(\frac{1}{\Delta}\sum_{\tau=t-\Delta}^{t} \varphi^{\text{out}}_i(\tau)\right) \cdot \left(\frac{1}{\Delta}\sum_{\tau=t-\Delta}^{t} \varphi^{\text{in}}_i(\tau)\right)}. \tag{13}$$

In Eq. (13), we consider only positive values of $\varphi^{\text{out}}_i(t)$ and $\varphi^{\text{in}}_i(t)$. This approach ensures that high values of $\mathcal{G}^i_{\text{net}}(t, \Delta)$ occur only when both the outflow of L agents and the inflow of M and H agents are substantial during the same period. Including negative values would erroneously indicate gentrification in areas where L agents replace M and H agents, which actually signals neighborhood impoverishment.

We define t_{peak} as the time of a gentrification event, corresponding to a local maximum in $\mathcal{G}^i_{\text{net}}(t, \Delta)$ or the onset of a plateau after rapid growth (see Sec. 6 for details).

To quantify gentrification at the city scale, we introduce two cumulative metrics: $\mathcal{G}^{\text{city}}_{\text{bin}}$, the percentage of nodes experiencing transitions in $\mathcal{G}_{\text{bin}}$, and $\mathcal{G}^{\text{city}}_{\text{net}}$, the percentage of nodes showing peaks in $\mathcal{G}_{\text{net}}$ (see Sec. 6 for details).

4. Results

4.1. *High-income agents drive gentrification*

We examine the impact of H agent mobility on gentrification dynamics. Simulations were conducted with varying H agent movement probabilities (p_H), while maintaining a fixed evaluation window of $\theta = 20$ time steps for node growth rates.

Figures 3(a) and 3(b) illustrate the influence of p_H on spatial gentrification patterns. With $p_H = 0$, both $\mathcal{G}^{\text{city}}_{\text{bin}}$ and $\mathcal{G}^{\text{city}}_{\text{net}}$ yield 0%, indicating complete absence of gentrification when H agents are static. Introducing minimal H agent mobility

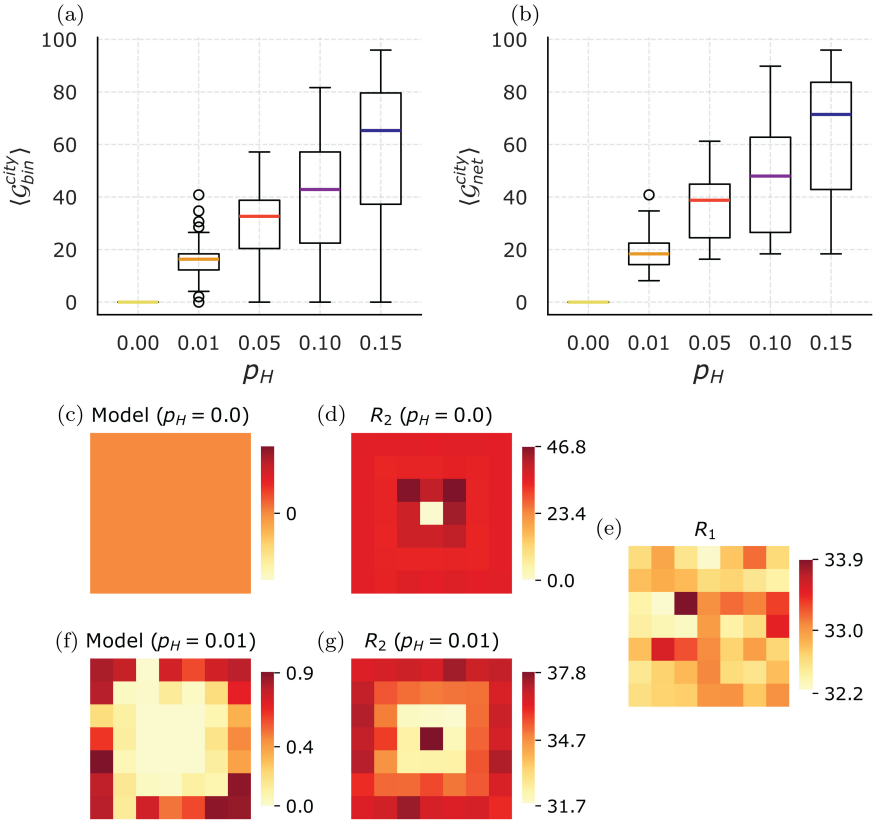

Fig. 3. (Color online) Gentrification patterns in our model: (a), (b) Gentrification level across 150 simulation of the model with a fixed $\theta = 20$, $N = 2^{12}$ and varying value of p_H according to $\mathcal{G}_{\text{bin}}^{\text{city}}$ (a) and to the network based measure $\mathcal{G}_{\text{net}}^{\text{city}}$ (b). (c)–(g) Heatmaps of the average number of peaks of $\mathcal{G}_{\text{net}}^{i}(t)$ observed in any neighborhood i over 150 simulations of our model (left), the R_2 null model (center) and the R_1 null model (right).

($p_H = 0.01$) triggers gentrification in 20%–40% of nodes, according to both metrics. This abrupt transition highlights the critical role of H agent mobility in initiating the gentrification process. As p_H increases, we observe a monotonic rise in gentrification levels, with $\mathcal{G}_{\text{bin}}^{\text{city}}$ and $\mathcal{G}_{\text{net}}^{\text{city}}$ showing similar trends but slightly different magnitudes.

To evaluate the significance of movement rules in driving gentrification, we compare our gentrification model with two null models: (i) R_1, where agents decide whether and where to relocate with a fixed probability (50%); (ii) R_2, where only the destination choice is random (details in Supplementary Information 1). Figures 3(c)–3(g) show heatmaps of the average $\mathcal{G}_{\text{net}}^{i}(t)$ peaks per neighborhood for the gentrification model and the two null models. Figure 3(c) highlights that no gentrification occurs in our model when $p_H = 0.0$, while gentrification events persist in the null models (Figs. 3(d) and 3(e)) even in the absence of H agents' movement.

Figure 3(f) show how, in our model, with $p_H = 0.01$, gentrification events are concentrated into peripheral neighborhoods dominated by L agents. In contrast, both null models (Figs. 3(e) and 3(g)) show widespread gentrification events, including cyclical transitions between L- and M-majority in central neighborhoods. Figure S1 further shows that none of the null models converge to stable configurations. The results indicate that the rules established by our model enhance the likelihood of gentrification occurring in neighborhoods that are initially low-income. This pattern is not observed in the null models, highlighting the significance of the rules we developed for generating gentrification events, in line with the definition of gentrification found in the literature [14, 48, 51].

4.2. *Network-based measure anticipates count-based measure*

While $\mathcal{G}_{\text{bin}}$ provides an intuitive measure of gentrification by capturing demographic transitions from L to M/H agent majorities, $\mathcal{G}_{\text{net}}$ enables earlier detection by identifying patterns of coordinated movement through temporal networks, revealing gentrification dynamics before visible demographic shifts occur. Figure 4(a) displays

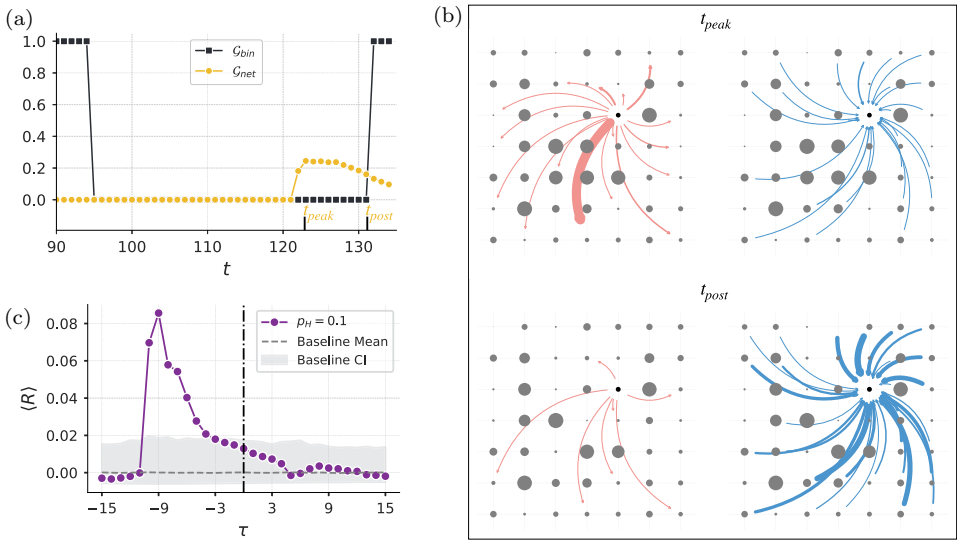

Fig. 4. (Color online) Evolution of a gentrification event for a representative node ($p_H = 0.1$, $\theta = 20$, $\Delta = 15$) and $N = 2^{12}$. (a) Comparison of $\mathcal{G}_{\text{net}}$ (in gold) and $\mathcal{G}_{\text{bin}}$ (in black) measures over time highlighting two key moments : during and after the peak in $\mathcal{G}_{\text{net}}$, i.e. t_{peak} and t_{post}, respectively. (b) Relocation in- and out-flows during (top), and after (bottom) the peak of $\mathcal{G}_{\text{net}}$. Red arrows correspond to L agent outflows, blue arrows correspond to M and H agent inflows within Δ, node size is proportional to agents population. (top) Peak: Simultaneous L outflow and $M + H$ inflow. (bottom) Post-peak: Diminishing L outflow, intensifying M and H inflow. Flows represent gross out- and in- strengths. (c) Average cross-correlation $\langle R \rangle$ between $\mathcal{G}_{\text{net}}$ and $\mathcal{G}_{\text{bin}}$ across all nodes and 150 model runs, as a function of lag τ. Gray area shows 95% confidence interval; dotted line indicates null distribution mean.

$\mathcal{G}_{\text{net}}(t, \Delta)$ and $\mathcal{G}_{\text{bin}}(t, \Delta)$ curves for a node in a representative simulation. In this example, the node initially experiences impoverishment, as $\mathcal{G}_{\text{bin}}$ transitions from 1 to 0 at approximately $t = 95$, indicating a shift from over- to under-representation of M and H residents. However, $\mathcal{G}_{\text{net}}$ shows a rapid increase at $t = 122$, followed by a plateau at $t = 123$, approximately 10 steps before the abrupt transition from 0 to 1 in $\mathcal{G}_{\text{bin}}$ at $t = 132$.

Figure 4(b) illustrates relocation dynamics during and after the $\mathcal{G}_{\text{net}}$ peak for the same node (neighborhood) analyzed in Fig. 4(a). Red arrows indicate L agent outflows, and blue arrows show $M + H$ inflows. At the peak (t_{peak}), both occur simultaneously, with more L agents leaving. After the peak, $M + H$ inflows increase while L outflows decrease. Unlike the gross flows in the visualization, $\mathcal{G}_{\text{net}}$ captures net flows, offering a more nuanced understanding of these changes.

To verify the consistency with which $\mathcal{G}_{\text{net}}$ peaks precede $\mathcal{G}_{\text{bin}}$ transitions across our simulations, we conduct a lagged cross-correlation analysis between $\mathcal{G}_{\text{net}}$ and $\mathcal{G}_{\text{bin}}$ time series. Specifically, we first compute the cross-correlation for each node in the city grid, then average these cross-correlations across all nodes. This process is repeated for 150 independent model runs, and the results are again averaged to obtain the final cross-correlation profile, reported in Fig. 4(c). We compute cross-correlations for lags $\tau \in [-15, +15]$ (see Sec. 6 for details), with significance tested against a null distribution. The highest correlation at $\tau = -9$ shows that $\mathcal{G}_{\text{net}}$ peaks systematically anticipate $\mathcal{G}_{\text{bin}}$ transitions by approximately 9 time steps. We further validate these findings repeating the analyses in the two randomized versions of the model. The anticipatory behavior of $\mathcal{G}_{\text{net}}$ relative to $\mathcal{G}_{\text{bin}}$ transitions disappears in both the fully random and random-destination versions of the model (see Fig. S2). This result supports our main findings, demonstrating that $\mathcal{G}_{\text{net}}$ reliably anticipates $\mathcal{G}_{\text{bin}}$ only in scenarios where agents' movements are influenced by their income distribution of in the city neighborhoods. More measures and parameter combination are provided in Supplementary Information 2.

We analyze the relationship between $\mathcal{G}_{\text{net}}$ and socioeconomic neighborhood dynamics in Fig. 5. Nodes exhibiting $\mathcal{G}_{\text{net}}$ peaks are color-coded, while those where $\mathcal{G}_{\text{net}}$ remains at zero are depicted in gray (Fig. 5(a)). We now consider the median of the income distribution of agents populating a neighborhood at a specific time as the *richness* of that neighborhood at that time. Richness time series reveal a starting trimodal distribution: high-richness central nodes (neighborhoods), intermediate-richness nodes, and low-richness nodes (Fig. 5(b)). Several nodes transition from low to intermediate richness, coinciding with $\mathcal{G}_{\text{net}}$ peaks. A notable exception (pink curve) displays a sharp richness increase followed by a steep decline, ultimately transitioning from low to middle richness. $\mathcal{G}_{\text{net}}$ correctly detects gentrification only after the moment this curve transitions from low to middle richness, disregarding the earlier fluctuations. The overall correspondence between the color-coded curves in both figures validates the capacity of $\mathcal{G}_{\text{net}}$ to identify gentrification solely based on relocation patterns.

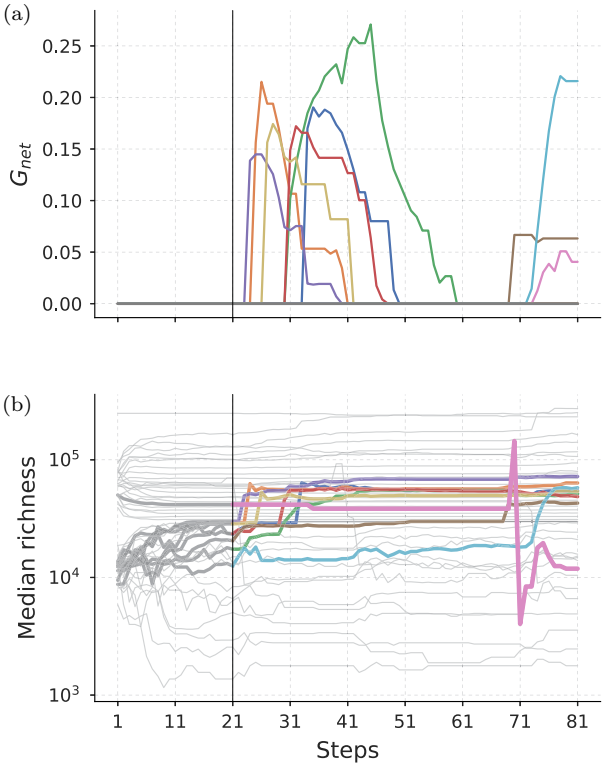

Fig. 5. (Color online) $\mathcal{G}_{\text{net}}$ peaks capture richness transitions in neighborhoods: (a) Time series of $\mathcal{G}_{\text{net}}(t, \Delta)$, with fixed values of the time window width $\Delta = 15$, of only the nodes that undergo sharp peaks of $\mathcal{G}_{\text{net}}$. (b) Time series of the richness (median of agents' income) of all nodes in the network: the colored curves correspond to the same nodes whose time series of $\mathcal{G}_{\text{net}}$ is presented in (a). The black vertical line in both plots indicates the initial time step when H agents become eligible to relocate, occurring θ steps after the simulation's start.

4.3. *Gentrification follows city density*

In Figs. 6(a)–6(c), we show the relationship between urban density and gentrification levels across different values of the model parameter p_H. We conduct 150 simulations for each configuration, with fixed values of the parameters $\theta = 20$ and $\Delta = 10$. To model increasing urban density, we run each simulation with a different number of agents (N) present in the grid, while keeping the grid dimension constant at 7×7 along with the capacity of individual nodes K.

City-wise gentrification levels, as captured by $\mathcal{G}_{\text{net}}^{\text{city}}$ (Fig. 6(a)) and $\mathcal{G}_{\text{bin}}^{\text{city}}$ (Fig. 6(b), is characterized by a clear trend: as city population density increases, so does the propensity for gentrification, in terms of number of gentrification events as observed by the two measures (see Sec. 6 for details), averaged over the different runs of the model. Furthermore, this effect is amplified by the H agents relocation rate p_H, as the curves in the two figures increase monotonically with N, with the exception of 0 or

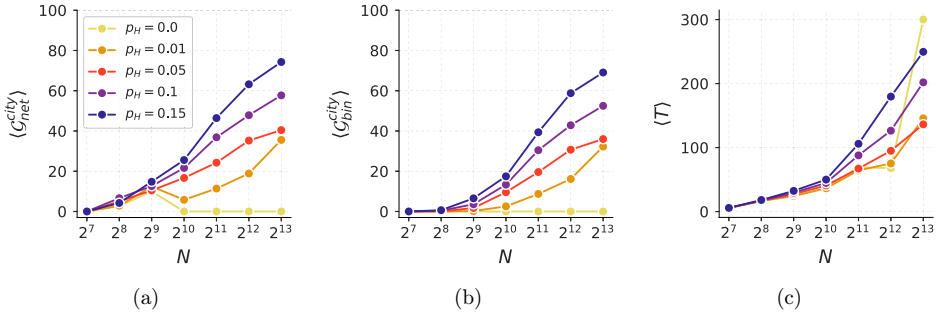

Fig. 6. (Color online) City density drives gentrification dynamics: Average results across 150 simulations for varying agent populations (x-axis, logarithmic scale) and high-income agent relocation rates p_H (colors). (a), (b) City-wise gentrification levels measured by $\mathcal{G}_{\text{net}}^{\text{city}}$ (a) and $\mathcal{G}_{\text{bin}}^{\text{city}}$ (b). (c) Number of average simulation time steps. Higher urban densities facilitate gentrification and increase convergences time.

very low values of p_H and low N for $\mathcal{G}_{\text{net}}$, as shown in Fig. 6(a). In Fig. 6(c), we show the relationship between city density and the average convergence time $\langle T \rangle$, the mean number of steps required to reach the termination condition over the 150 simulations, where L agents can no longer move. The average convergence time $\langle T \rangle$ increases with both N and p_H, except when $p_H = 0$. In this case, where H agents are present but stationary and the city is extremely dense, the model does not reach the termination condition within the imposed 300-step limit when $N \geq 2^{13}$.

In addition to city-level dynamics, neighborhood density, limited by fixed capacity, plays an interesting role. In particular, we observe that the initially less populated low-income neighborhoods become increasingly crowded over time. This is driven by the displacement pressure exerted by higher-income agents, who push lower-income agents out of more desirable areas. As a result, low-income agents concentrate into a few affordable neighborhoods, leading to significant overcrowding. A detailed analysis of this process is provided in Supplementary Information 5.

Overall, these results suggest how higher urban densities lead to the emergence of more gentrification waves throughout the evolution of a city.

5. Discussion

Our study introduces an agent-based model of gentrification that categorizes inhabitants of a city into three income groups – low, medium and high – and simulates agent movements within a grid-based urban environment driven by socioeconomic factors. The model effectively captures the essence of gentrification dynamics, consisting in the displacement of lower income inhabitants of a neighborhood of the city caused by a simultaneous inflow of wealthier citizens [14]. This characteristic of gentrification is evidenced by the results of our simulations and quantitatively described by our proposed network-based measure.

We find that even a small proportion of high-income agents (5% of the population) significantly affect the dynamics of gentrification. When high-income agents do

not move, even if still present in the model city, no gentrification is detected, and the model does not converge within the imposed limit of 300 steps. However, introducing even a low probability for the movement of high-income agents ($p_H = 1\%$) leads to model convergence in approximately 150 steps, while 40% of the city neighborhoods experience at least one gentrification wave. Interestingly, when the model is initialized with a random configuration in which agents of all three types are substantially represented in each neighborhood (see Figs. S10–S13), rather than with a core-periphery structure, it rapidly converges to a segregated state. This outcome is equivalent to the final configuration obtained in simulations starting from the core-periphery setup, although it lacks any preserved spatial organization.

Our measures, $\mathcal{G}_{\text{count}}$ and $\mathcal{G}_{\text{net}}$, represent two distinct approaches to quantify gentrification. The count-based measure $\mathcal{G}_{\text{count}}$ evaluates the concentration of agents of the three types in each neighborhood over a time window Δ. A significance threshold ($n^*_{H,M}$) is needed to detect when middle- and high-income agents are over-represented and, therefore, define the binarized version of the count-based measure, $\mathcal{G}_{\text{bin}}$. Such measure thus captures neighborhood transitions from under- to over-representation of middle- and high-income agents, indicating the completion of gentrification. The network-based measure $\mathcal{G}_{\text{net}}$ tracks the net inflow of middle- and high-income agents and the simultaneous outflow of lower-income agents over Δ. This measure is thus rooted in temporal network analysis, where the existence of structures [9, 24, 42] in the networks under study is related to the simultaneity of the interactions (edges) between pairs or groups of nodes. Furthermore, this network-based approach avoids more or less arbitrary thresholds and aligns with available commuting flow data [4, 33, 37, 40], which could serve as a proxy given the absence of residential relocation records. $\mathcal{G}_{\text{net}}$ helps identifying early signs of gentrification by tracking peaks or plateaus in its trajectory, correlating higher-income resident influx with lower-income displacement. The cross-correlation computed between the count-based and the network-based measures highlights how peaks in $\mathcal{G}_{\text{net}}$ are consistently and significantly observed in advance with respect to $\mathcal{G}_{\text{count}}$. The analysis of the randomized versions of our model, in Supplementary Information 1, shows that while gentrification events caused by random agent-relocations are still detected, no significant cross-correlation exists between our two measures, emphasizing the importance of the agents' decision-making rules in our model for predicting transitions. Our results hold true also when relaxing the termination condition of our model, thus allowing longer simulations (Supplementary Information 8). Furthermore, the analyses of longer simulations reveal a quasi-periodic occurrence of gentrification waves, defined as peaks of the time series of the volume of gentrification events unfolding across the whole city. These results demonstrate that our minimal model captures the essential features needed to reproduce gentrification: a heavy-tailed income distribution, few income classes, and distinct relocation strategies — notably the profit-driven behavior of high-income agents. Moreover, our network-based measure $\mathcal{G}_{\text{net}}$ enables earlier detection of gentrification compared to count-based metrics, potentially aiding policymakers in preventing low-income

displacement.

While our model provides valuable insights into gentrification dynamics, it has limitations that future research could address. The constant population size and static income-group assignments could be expanded to incorporate population growth and inter-city migration flows, potentially using a network-based approach to disentangle endogenous and exogenous causes of gentrification [21]. With the implementation of these extensions of our model, a complementary measure of impoverishment of a neighborhood, such as the one we propose in the Supplementary Material (Supplementary Material 7) could help elucidate, in a quantitative manner, the causal relationships between the periods of impoverishment/disinvestment and gentrification of neighborhoods. Multiple property ownership per agent could be introduced to model wealth concentration and short-term rental effects. The grid-based urban representation could be enhanced with more complex geographical features, although our results hold for both 7×7 and 9×9 grids (Supplementary Information 3). Moreover, simulating policy interventions [34] could provide insights for urban planners, particularly regarding density restrictions given our findings on city density and gentrification probability.

In conclusion, our agent-based model and novel quantitative measures offer a powerful framework for understanding and predicting gentrification processes. This approach not only advances our theoretical understanding of gentrification but also provides quantitative what-if tools for early detection and potential mitigation of its effects in real-world urban environments.

6. Methods

6.1. *Agents' income*

At the beginning of a simulation, each agent is assigned a fixed income w, based on data from the 2022 USA Social Security Administration report [52]. The assignment process uses the income brackets and population percentages provided in this report. Each agent is assigned to an income bracket with probability proportional to the US population within that bracket, and then the agent's specific income w is randomly selected from within their assigned bracket. Agents are categorized into three groups based on their assigned incomes: L (low-income) agents with incomes up to \$29,999.99, encompassing the 2022 poverty line for a family of four (\$27,750); H (high-income) agents representing the top 5% of earners; and M (middle-income) agents comprising all remaining individuals.

6.2. *Gentrification: Peaks, shifts and aggregate measure*

A cell i undergoes gentrification events according to $\mathcal{G}_{\text{bin}}$ at all times t where there is a binary shift from 0 to 1 in the time series throughout the simulation:

$$T^i_{\text{shift}} = \{t : \mathcal{G}^i_{\text{bin}}(t, \Delta) = 1 \wedge \mathcal{G}^i_{\text{bin}}(t-1, \Delta) = 0\}. \tag{14}$$

A cell i undergoes gentrification events according to $\mathcal{G}_{\text{net}}$ at all times t where there is a peak in its time series throughout the simulation. A peak is defined as either a local maximum or the start of a plateau after a growing phase:

$$T^i_{\text{peak}} = \left\{ t : \begin{bmatrix} (\mathcal{G}^i_{\text{net}}(t,\Delta) > \mathcal{G}^i_{\text{net}}(t-1,\Delta) \wedge \mathcal{G}^i_{\text{net}}(t,\Delta) > \mathcal{G}^i_{\text{net}}(t+1,\Delta)) \\ \vee \\ (\mathcal{G}^i_{\text{net}}(t,\Delta) > \mathcal{G}^i_{\text{net}}(t-1,\Delta) \wedge \mathcal{G}^i_{\text{net}}(t,\Delta) = \mathcal{G}^i_{\text{net}}(t+1,\Delta)) \end{bmatrix} \right\}. \quad (15)$$

We define the gentrification level of the city as the percentage of cells of the city that experience at least one gentrification event according to each measure:

$$\mathcal{G}^{\text{city}}_{\text{bin}} = \frac{\sum_{i=1}^{N_{\text{cells}}} \mathbf{1}(|T^i_{\text{shift}}| > 0)}{N_{\text{cells}}} \times 100, \quad \mathcal{G}^{\text{city}}_{\text{net}} = \frac{\sum_{i=1}^{N_{\text{cells}}} \mathbf{1}(|T^i_{\text{peak}}| > 0)}{N_{\text{cells}}} \times 100, \quad (16)$$

where $\mathbf{1}(\cdot)$ is the indicator function.

6.3. *Lagged cross-correlation*

We compute the mean cross-correlation $\langle R \rangle$ by calculating the lagged cross-correlation between pairs of time series of $\mathcal{G}^i_{\text{net}}(t,\Delta)$ and $\mathcal{G}^i_{\text{bin}}(t,\Delta)$ corresponding to each cell on the grid-view of a model city, for several values of the lag τ, and then averaging over all cells. To compute the cross-correlation R^i between the two time series for a cell i, we transform the two time series into two binary vectors (see Supplementary Information 4 for further details) $\tilde{\mathcal{G}}^i_{\text{net}}$ and $\tilde{\mathcal{G}}^i_{\text{bin}}$ of length T, where the t_kth entry is 1 if the original corresponding time series has a peak or 0–1 transition at time $t_k \in [0,T]$, respectively:

$$(\tilde{\mathcal{G}}^i_{\text{net}})_{t_k} = \begin{cases} 1, & \text{if } t_k \in T^i_{\text{peak}}, \\ 0, & \text{otherwise}, \end{cases} \quad (17)$$

$$(\tilde{\mathcal{G}}^i_{\text{bin}})_{t_k} = \begin{cases} 1, & \text{if } t_k \in T^i_{\text{shift}}, \\ 0, & \text{otherwise}. \end{cases} \quad (18)$$

For each value of the lag $\tau \in [-15,+15]$, we compute the lagged cross-correlation between the two vectors and obtain a value of $R^i(\tau)$ for each cell i on the grid. We then calculate $\langle R \rangle$ by averaging, for each value of the lag τ, the values of $R^i(\tau)$ over all cells $i \in [0, N_{\text{cells}}]$:

$$\langle R(\tau) \rangle = \frac{\sum_{i \in [0,N_{\text{cells}}]} R^i(\tau)}{N_{\text{cells}}}. \quad (19)$$

To establish a baseline for comparison, we generate a null distribution by computing, for each cell i, the cross-correlation R between 50 pairs of randomly reshuffled versions of the two vectors $\tilde{\mathcal{G}}^i_{\text{net}}$ and $\tilde{\mathcal{G}}^i_{\text{bin}}$.

Code Availability Statement

The code for the implementation of our model and to reproduce our analyses can be found at https://github.com/mauruscz/Gentrification.

Acknowledgments

We thank Daniele Fadda for its precious support with the visualizations. We thank Dino Pedreschi, Timothy LaRock, Rohit Sahasrabuddhe, Andrea Beretta, Giuliano Cornacchia, Margherita Lalli, Daniele Gambetta, Emanuele Ferragina and Salvatore Citraro for their useful suggestions. This work has been partially supported by: EU project H2020 SoBigData++ G.A. 871042; PNRR (Piano Nazionale di Ripresa e Resilienza) in the context of the research program 20224CZ5X4 PE6 PRIN 2022 "URBAI — Urban Artificial Intelligence" (CUP B53D23012770006), funded by the European Commission under the Next Generation EU programme; and by PNRR — M4C2 — Investimento 1.3, Partenariato Esteso PE00000013 — "FAIR — Future Artificial Intelligence Research" — Spoke 1 "Human-centered AI", funded by the European Commission under the NextGeneration EU programme; project "SoBigData.it — Strengthening the Italian RI for Social Mining and Big Data Analytics", prot. IR0000013, avviso n. 3264 on 28/12/2021. NP and RL received funding from EPSRC Grant Ref EP/V013068/1.

Author Contributions

GM: study conceptualization, model implementation, experiment design, execution of experiments, code implementation, interpretation of results, writing, plots and images, study management. NP: study conceptualization, model implementation, experiment design, interpretation of results, writing, plots design. LP: study conceptualization, experiment design, interpretation of results, writing, study direction. RL: study conceptualization, experiment design, interpretation of results, writing, study direction. All authors read and approved the final manuscript.

Supplementary Material

The supplementary materials are available at: https://www.worldscientific.com/doi/suppl/10.1142/S0219525925400065

ORCID

Giovanni Mauro https://orcid.org/0000-0001-8067-984X
Nicola Pedreschi https://orcid.org/0000-0003-1582-6246
Renaud Lambiotte https://orcid.org/0000-0002-0583-4595
Luca Pappalardo https://orcid.org/0000-0002-1547-6007

References

[1] Abel, G. J. and Cohen, J. E., Bilateral international migration flow estimates for 200 countries, *Sci. Data* **6** (2019) 82.

[2] Arribas-Bel, D. and Sanz-Gracia, F., The validity of the monocentric city model in a polycentric age: US metropolitan areas in 1990, 2000 and 2010, *Urban Geogr.* **35** (2014) 980–997.
[3] Banabak, S., Kadi, J. and Schneider, A. E., Gentrification and the suburbanization of poverty: Evidence from a highly regulated housing system, *Urban Geogr.* **45** (2024) 1596–1618.
[4] Barbosa, H., Barthelemy, M., Ghoshal, G., James, C. R., Lenormand, M., Louail, T., Menezes, R., Ramasco, J. J., Simini, F. and Tomasini, M., Human mobility: Models and applications, *Phys. Rep.* **734** (2018) 1–74.
[5] Barrat, A., Barthélemy, M., Pastor-Satorras, R. and Vespignani, A., The architecture of complex weighted networks, *Proc. Natl. Acad. Sci.* **101** (2004) 3747–3752, doi: 10.1073/pnas.0400087101.
[6] Barthelemy, M., *The Structure and Dynamics of Cities* (Cambridge University Press, 2016).
[7] Batty, M., *The New Science of Cities* (The MIT Press, 2013).
[8] Christafore, D. and Leguizamon, S., Neighbourhood inequality spillover effects of gentrification, *Papers Region. Sci.* **98** (2019) 1469–1485.
[9] Ciaperoni, M., Galimberti, E., Bonchi, F., Cattuto, C., Gullo, F. and Barrat, A., Relevance of temporal cores for epidemic spread in temporal networks, *Sci. Rep.* **10** (2020) 12529, doi: 10.1038/s41598-020-69464-3.
[10] Cornacchia, G., Böhm, M., Mauro, G., Nanni, M., Pedreschi, D. and Pappalardo, L., How routing strategies impact urban emissions, in *Proc. 30th Int. Conf. Advances in Geographic Information Systems (SIGSPATIAL '22)* (Association for Computing Machinery, New York, NY, USA, 2022), Article 42, pp. 1–4.
[11] Eckerd, A., Kim, Y. and Campbell, H., Gentrification and displacement: Modeling a complex urban process, *Housing Policy Debate* **29** (2019) 273–295.
[12] Gambetta, D., Mauro, G. and Pappalardo, L., Mobility constraints in segregation models, *Sci. Rep.* **13** (2023) 12087.
[13] Gardiner, O. and Dong, X., Mobility networks for predicting gentrification, in *Complex Networks & Their Applications IX: Volume 2, Proceedings of the Ninth International Conference on Complex Networks and Their Applications COMPLEX NETWORKS 2020* (Springer, 2021), pp. 181–192.
[14] Glass, R., Aspects of change, in *The Gentrification Debates* (Routledge, 2013), pp. 19–29.
[15] Gueuning, M., Cheng, S., Lambiotte, R. and Delvenne, J.-C., Rock–paper–scissors dynamics from random walks on temporal multiplex networks, *J. Compl. Netw.* **8** (2020) cnz027.
[16] Hamnett, C., Gentrification, postindustrialism, and industrial and occupational restructuring in global cities, in *A Companion to the City*, eds G. Bridge and S. Watson (2000), pp. 331–341.
[17] Holme, P., Modern temporal network theory: A colloquium, *Eur. Phys. J. B* **88** (2015) 234.
[18] Holme, P. and Saramäki, J., Temporal networks, *Phys. Rep.* **519** (2012) 97–125.
[19] Hu, M., Tsang, D. and Wan, W. X., Corporate relocation and housing market spillovers, *Manag. Sci.* **71** (2024) 4344–4376.
[20] Jacobs, J., *The Death and Life of Great American Cities* (Random House, New York, 1961).
[21] Janssen, K. M. J., Cottineau-Mugadza, C., Kleinhans, R. and van Bueren, E., Spatial dynamics of incoming movers and the state-led gentrification process: The case of rotterdam, *Popul. Space Place* **30** (2024) e2851, doi: 10.1002/psp.2851.

[22] Kazil, J., Masad, D. and Crooks, A., Utilizing python for agent-based modeling: The mesa framework, in *Social, Cultural, and Behavioral Modeling*, eds. Thomson, R., Bisgin, H., Dancy, C., Hyder, A. and Hussain, M. (Springer International Publishing, Cham, 2020), pp. 308–317.
[23] Kivelä, M., Arenas, A., Barthelemy, M., Gleeson, J. P., Moreno, Y. and Porter, M. A., Multilayer networks, *J. Compl. Netw.* **2** (2014) 203–271, doi: 10.1093/comnet/cnu016.
[24] Kobayashi, T., Takaguchi, T. and Barrat, A., The structured backbone of temporal social ties, *Nature Commun.* **10** (2019) 220.
[25] LeRoy, S. F. and Sonstelie, J., Paradise lost and regained: Transportation innovation, income, and residential location, *J. Urban Econ.* **13** (1983) 67–89.
[26] Ley, D., Artists, aestheticisation and the field of gentrification, *Urban Stud.* **40** (2003) 2527–2544.
[27] Lipton, S. G., Evidence of central city revival, *J. Amer. Plan. Assoc.* **43** (1977) 136–147.
[28] Liu, C. and O'Sullivan, D., An abstract model of gentrification as a spatially contagious succession process, *Comput. Environ. Urban Syst.* **59** (2016) 1–10.
[29] Lowry, I. S., Filtering and housing standards: A conceptual analysis, *Land Econ.* **36** (1960) 362–370.
[30] Lucchini, L., Centellegher, S., Pappalardo, L., Gallotti, R., Privitera, F., Lepri, B. and De Nadai, M., Living in a pandemic: Changes in mobility routines, social activity and adherence to COVID-19 protective measures, *Sci. Rep.* **11** (2021) 24452.
[31] Mantzaris, A. V., Incorporating a monetary variable into the Schelling model addresses the issue of a decreasing entropy trace, *Sci. Rep.* **10** (2020) 17005.
[32] Masuda, N. and Lambiotte, R., *A Guide to Temporal Networks* (World Scientific, 2016).
[33] Mauro, G., Luca, M., Longa, A., Lepri, B. and Pappalardo, L., Generating mobility networks with generative adversarial networks, *EPJ Data Sci.* **11** (2022) 58.
[34] Mauro, G. and Pappalardo, L., The role of relocation policies in urban segregation dynamics, in *EDBT/ICDT Workshops*, Paestum, Italy, (2024) Article 7, pp. 1–8.
[35] Moro, E., Calacci, D., Dong, X. and Pentland, A., Mobility patterns are associated with experienced income segregation in large US cities, *Nature Commun.* **12** (2021) 4633.
[36] Nieuwenhuis, J., Tammaru, T., Van Ham, M., Hedman, L. and Manley, D., Does segregation reduce socio-spatial mobility? Evidence from four European countries with different inequality and segregation contexts, *Urban Stud.* **57** (2020) 176–197.
[37] Noulas, A., Scellato, S., Lambiotte, R., Pontil, M. and Mascolo, C., A tale of many cities: Universal patterns in human urban mobility, *PloS One* **7** (2012) e37027.
[38] Oliver, N. *et al.*, Mobile phone data for informing public health actions across the COVID-19 pandemic life cycle, *Science Advances* **6** (2020) eabc0764.
[39] O'Sullivan, D., Toward micro-scale spatial modeling of gentrification, *J. Geogr. Syst.* **4** (2002) 251–274.
[40] Pappalardo, L. *et al.*, A survey on the impact of AI-based recommenders on human behaviours: Methodologies, outcomes and future directions, arXiv:2407.01630.
[41] Pappalardo, L., Manley, E., Sekara, V. and Alessandretti, L., Future directions in human mobility science, *Nature Comput. Sci.* **3** (2023) 588–600.
[42] Pedreschi, N., Battaglia, D. and Barrat, A., The temporal rich club phenomenon, *Nature Phys.* **18** (2022) 931–938.
[43] Reades, J., De Souza, J. and Hubbard, P., Understanding urban gentrification through machine learning, *Urban Stud.* **56** (2019) 922–942.
[44] Redfern, P. A., A new look at gentrification: 2 a model of gentrification, *Environ. Plan. A* **29** (1997) 1335–1354.

[45] Rigolon, A. and Németh, J., Toward a socioecological model of gentrification: How people, place, and policy shape neighborhood change, *J. Urban Affairs* **41** (2019) 887–909.
[46] Schelling, T. C., Dynamic models of segregation, *J. Math. Soc.* **1** (1971) 143–186.
[47] Shaw, J. D., Restrepo, J. G. and Rodríguez, N., A dynamical system model of gentrification: Exploring a simple rent control strategy, arXiv:2406.12092.
[48] Simpson, J., Planning gentrification, *Planning* (2017).
[49] Slater, T., Gentrification of the city, in *The New Blackwell Companion to the City*, eds G. Bridge and S. Watson (2011), pp. 571–585.
[50] Smith, N., Toward a theory of gentrification a back to the city movement by capital, not people, *J. Amer. Plan. Assoc.* **45** (1979) 538–548.
[51] Smith, N., Gentrification and the rent gap, *Ann. Assoc. Amer. Geogr.* **77** (1987) 462–465.
[52] Social Security Administration, 2022 compensation data (2022). Available at https://www.ssa.gov/cgi-bin/netcomp.cgi?year=2022 [Accessed on 2024-09-11].
[53] Torrens, P. M. and Nara, A., Modeling gentrification dynamics: A hybrid approach, *Comput. Environ. Urban Syst.* **31** (2007) 337–361.